Indian Journal of Chemical Technology
Vol. 31, November 2024, pp. 902-913
DOI: 10.56042/ijct.v31i6.10398

Simulation of natural convection in a square cavity with micropolar fluid and magnetic fields using FVM

N. Vinodhini[1]* & V. Ramachandra Prasad[2]*

[1]Department of Mathematics, Saveetha Engineering College, Chennai-602 105, Tamil Nadu, India

[2]Department of Mathematics, School of Advances Sciences, Vellore Institute of Technology, Vellore 632 014, Tamil Nadu, India

*E-mail: vinodhini9208@gmail.com

Received 13 April 2024; accepted 9 September 2024

This paper investigates the heat and mass transfer characteristics of micropolar nanofluid contained within an enclosure subjected to buoyancy force and magnetic field. The mathematical model is developed using governing equations mass, energy, and momentum to assess the thermal efficiency of micropolar fluid. The objective of this research is to enhance the effectiveness of heat and mass transfer in industrial heat transfer devices and heat recovery systems utilized in engineering processes. The considered numerical study visualizes the magnetic hydrodynamic effect in two-dimensional natural convection heat transfer occurring from a square enclosure. The fluid inside the enclosure travels in a laminar pattern, incompressible and time-dependent. The research deals with micropolar fluid characterized by its Prandtl number (Pr=0.71). The horizontal magnetic field is utilized in the system. To discretize the nonlinear paired dimensionless boundary value problem the computation technique known as Versteeg and Malalasekera Finite Volume Method (FVM) is used.The graphical representation illustrates the influence of crucial control parameters on streamline contours, isotherm contours, and local Nusselt numbers. The convective flow and heat transfer within the cavity are affected by an elevation in the vortex viscosity parameter. As a result, the streamlines and isotherms are largely invariant to a change in magnetic field orientation. Moreover, it has been found, that the higher Rayleigh numbers may induce vortices and eddies, creating secondary flow structures that enhance heat transfer and also the stronger buoyancy forces, driving more significant fluid motion and convective heat, resulting in more pronounced variations in temperature. Also, the study investigates how the placement of heat sources and the configuration of multiple heat sources impact the system, aiming to provide qualitative recommendations for enhancing cooling system design.

Keywords: Finite volume method, Micropolar fluid, MHD effect, Natural convection, Square enclosure

Introduction

Micropolar fluids have garnered significant attention from researchers due to their diverse applications in industries such as manufacturing, engineering, and technology. Unlike Newtonian fluids, microscopic fluids exhibit enhanced resistance to fluid motion. Moreover, it has been observed that a higher micropolar parameter value in fluid flow contributes to increased overall viscosity. Micropolar fluids are identified as the most suitable medium for laminar flow in various physical phenomena. Eringen[1] introduced the theory of micropolar fluids, which focuses on describing the flow of fluids containing micro-constituents that undergo rotation. Eringen's work on micropolar fluids was further extended to include thermo-micropolar fluids, exploring the microscopic effects and micro-motion resulting from the local arrangement of fluid components. The micropolar fluid theory, proposed by Eringen, provides a framework for comparing with other fluid models, both non-Newtonian and Newtonian. This theory delves into the study of liquid particle rotation by incorporating an independent kinematic vector known as the microrotation vector.

Saleem *et al.*[2] conducted a numerical investigation on convection energy transfer within a micropolar fluid confined in a rectangular enclosure with heated and cooled lower boundaries. The study considered various values of Prandtl number, Rayleigh number, vortex viscosity parameter, and cavity length. The researchers analyzed the flow patterns and their impact on heat transfer and skin friction. The findings revealed that, under identical physical conditions, the heat transfer rate from a heated surface in a micropolar fluid is lower compared to that in a Newtonian fluid. Gibanov *et al.*[3] explored the natural convective flow and heat transfer of a micropolar fluid in a wavy differentially heated chamber, noting that an increase in the vortex viscosity parameter (K) leads to an augmentation in microrotation. Zadravec *et al.*[4] employed a boundary

element approach to study natural convection of micropolar fluid in an enclosure. Their work focused on numerical simulations of natural convection in micropolar fluids, specifically examining the flow of suspensions with particles that rotate independently. The results demonstrated that the micro-rotation of particles in a general suspension diminishes overall heat transfer from the hot wall. This aspect should not be overlooked when estimating the heat and fluid flow characteristics of micropolar fluids.

Sheikholeslami *et al*.[5] employed the homotopy perturbation method (HPM) to analyze micropolar fluid flow and heat transfer in a permeable channel. HPM, a technique for solving nonlinear equations, was briefly explained and utilized to find solutions. A comparison was made with numerical results obtained using the Runge–Kutta method of order 4. In the context of micropolar fluids, incorporating a transport equation for local angular momentum conservation is essential. This requires introducing new local constitutive parameters in addition to the standard equations for mass and momentum conservation. Javed and Siddiqui[6] explored mixed convective energy flow in a square container filled with micropolar fluid under the influence of a constant horizontal magnetic field. The study revealed that the frequency of streamlined circulations increased with the Grash of (Gr) number but decreased with the Hartmann (Ha) and Reynolds (Re) numbers. Sheremet *et al.*[7] conducted a numerical analysis of natural convection in a right-angled wavy triangular cavity filled with micropolar fluid. Utilizing the Boussinesq approximation, governing equations were developed in dimensionless stream function, vorticity, and temperature.

Ariman *et al*.[8] emphasized the utilization of micro continuum fluid mechanics in various applications, including fluids with rigid non-spherical or deformable microelements, micropolar fluids, polar and dipolar fluids, couple stress fluids, anisotropic fluids, and liquid crystals. In the above-mentioned two comprehensive articles, the distinctive characteristics of micropolar fluids were thoroughly examined, and the practical applications of this theory were explored. Yashida and Hamano[9] conducted a numerical study on the dynamics of two-layer Rayleigh-Benard convection with an infinite Prandtl number and significant viscosity contrasts. Their research delved into the distinctive features of this convection phenomenon. Tso *et al.*[10] presented an investigation on the evolution of natural convection cooling flow patterns in a rectangular cavity with discrete heat sources at various orientations. They employed numerical simulations in both 2-D and 3-D, illustrating the development of flow and temperature patterns at different inclination angles.

Aydın and Pop[11] conducted an experimental study on natural convection within a differentially heated enclosure filled with micropolar fluid. Frederick[12] statistically investigated natural convection in a differently heated inclined square enclosure with a fin connected to the cold vertical wall. Bilgen[13] performed numerical simulations on natural convection heat transport in a differentially heated chamber with a horizontal fin attached to the hot wall, demonstrating the significant impact of fin location on heat transport within the cavity. In a previous study by Hsu[14] natural convection of micropolar fluids in a heat-generating enclosure was explored, considering single or multiple uniform heat sources. The effects of heat source locations and various arrangements were examined to provide insights for improving the cooling design of the system. Gibanov *et al.*[15] discussed free convection in a trapezoidal chamber filled with micropolar fluid, highlighting that an increase in the vortex viscosity parameter reduces convective flow and heat transfer inside the cavity. Miroshnichenko *et al.*[16] investigated natural convection of micropolar fluid flow in a trapezoidal cavity, emphasizing the impact of local heat sources. The computations involved relevant parameters such as Prandtl number, Rayleigh number, and vortex viscosity parameter. Basak *et al.*[17] presented the flow of natural convection within a square enclosure with uniform and non-uniform heated walls. Khanafer *et al.*[18] analyzed unsteady mixed convection in a driven cavity using an externally excited sliding lid.

Over the past decade, there has been significant progress in the application of numerical methods to simulate various complex medical problems, particularly those involving intricate geometries. Researchers have primarily employed the finite element method (FEM) and the finite volume method (FVM) for these simulations. The FVM, known for its flexibility in handling diverse control modules and unstructured meshes, has gained widespread use. Despite advancements, generating unstructured meshes for complex geometries remains a time-consuming challenge, prompting ongoing research efforts. A promising solution to this challenge involves the use of Octree meshes, which offer

advantages in processing resources and data structure. The Octree approach utilizes normal cubes (volumes) to represent intricate geometries, refining only in areas requiring higher resolution while describing others with larger volumes, resulting in a nonconforming mesh. Researchers are particularly interested in leveraging FVM to construct computational models with complex geometries. Barth[19] explained the significance of unstructured grids for Navier Stokes Equations using finite volume. Huang *et al.*[20] introduced an advanced finite volume method for solving non-conservative convection equations on unstructured meshes. Their approach tackles both a linear advection equation in its non-conservative form and a time-dependent eikonal equation. Nishikawa[21] addressed the prevailing confusion surrounding the QUICK system (Quadratic Upwind Interpolation for Convective Kinematics), specifically whether it qualifies as a second-order or third-order scheme. The paper serves as a definitive reference, aiming to eliminate any ambiguity regarding the third-order accuracy of the QUICK scheme. Additionally, it lays the groundwork for clarifying the principles behind cost-effective high-order unstructured-grid schemes, a topic to be further discussed in a subsequent paper. In a related study, Patel[22] delved into the examination of unsteady state convection-diffusion flow using the finite volume scheme. Busto *et al.*[23] explored Thermodynamically Compatible Finite Volume Methods and Path-Conservative ADER Discontinuous Galerkin Schemes for Turbulent Shallow Water Flows. Cao and Huang [24] investigated a Moving Mesh with an Adaptive Conservative Finite Volume Method for Poisson-Nernst-Planck (PNP) Equations. To enhance numerical solution accuracy, two innovative monitor functions were proposed for moving mesh partial differential equations, supplementing the conventional ones. Durlofsky *et al.*[25] introduced an adaptive local–global scheme for two-phase simulations, employing a multiscale finite volume technique. This method enables the efficient integration of approximate global information derived from coarse-scale simulations into multiscale basis functions. The approach is formulated as a finite volume element method and applied to simulate single- and two-phase flow in channelized two-dimensional systems. Balaji *et al.*[26] explored the energy-efficient system under a nanofluid-based intercooler. Prakash *et al.* [27] investigated the heat transmission effect of nanofluid under natural convection.

Acharya and Oztop[28] analyzed entropy and hydrothermal behavior of buoyancy-driven magnetized hybrid nanofluid flow in a semi-circular chamber equipped with a triangular heater: Implications for thermal energy storage in energy management applications. Acharya[29] studied the flow patterns and thermal regulation of radiative in natural convective hybrid nanofluid flow within a square enclosure featuring multiple heated obstacles of different shapes. Also, Acharya[30] researched the hybrid nanofluidic transport in magnetically driven force. From the aforementioned articles, it is noted that the Natural convection within a closed square cavity has been a focal point in numerous fundamental heat transfer analyses, playing a critical role in various technological applications. Indeed, buoyancy-induced convection within a sealed cavity featuring differentially heated isothermal walls serves as a prototype for numerous industrial applications. These include the energy-efficient design of buildings and rooms, the safe and efficient operation of nuclear reactors, and convective heat transfer processes associated with boilers.

In the literature review discussed earlier section of this manuscript, it is evident that the exploration of micropolar fluid dynamics has garnered considerable interest among researchers, particularly in engineering fields. In the present research, the selection of a Prandtl number of 0.71 (representative of gases) for micropolar fluids is likely based on a combination of experimental data, theoretical considerations, numerical stability requirements, and comparisons with similar studies. This choice ensures that the numerical simulation accurately represents the heat transfer behaviour of micropolar fluids under the specified conditions. Building on this background, the current investigation focuses on numerically simulating natural convection in a square enclosure filled with micropolar fluid, with an unsteady state incorporating both Magnetohydrodynamics (MHD) effects and the Boussinesq approximation. Notably, this study introduces a novel approach by considering the combined influences of these effects with an unsteady state filling a gap in existing research. This comprehensive approach contributes to a deeper understanding of how electronic devices, such as microprocessors in computers or electronic components in mobile devices, generate heat during operation. Efficient cooling systems are essential to dissipate this heat and prevent overheating, which can

lead to performance degradation or even component failure. By studying the heat transfer characteristics of micropolar fluids under the influence of MHD in a confined cavity, researchers can gain insights into how to optimize cooling systems to enhance heat dissipation in electronic devices. This understanding can aid in the development of innovative cooling technologies that improve thermal management and increase the reliability and performance of electronic devices in real-world applications.

Mathematical Formulation

Problem configuration

List of relevant non-dimensional parameters is shown in Table 1. The illustrated physical model is the ongoing investigation of applying Boussinesq approximation with micropolar effect. Consider the system is unsteady and the working fluid is laminar, incompressible, and natural convective flow of micropolar fluid in a two-dimensional square enclosure as shown in Fig. 1. The enclosure is a square with vertical walls and horizontal walls, each having a length of L. The top and bottom boundaries of the enclosure are thermally insulated, while the vertical boundaries are subjected to varying temperatures. The investigation of micropolar fluid flow in MHD is considered. The framework utilizes a horizontal magnetic field and the gravitational force g acting downwards of the domain. The working model employs the Boussinesq approximation, which assumes that density differences are negligible except in the buoyancy term of the momentum equation. This simplification allows the model to account for variations in density only where they affect gravitational forces, making it easier to analyze fluid flow and heat transfer.

Table 1 — List of relevant non-dimensional parameters

Prandtl number	Pr	$\frac{\nu}{\alpha}$
Hartman nnumber	Ha	$B_0 L\sqrt{\frac{\sigma}{\mu}}$
Rayleigh number	Ra	$\frac{g\beta(T_h - T_c)L^3}{(\alpha\gamma)}$
Vortex Viscosity Parameter	K	$\frac{k}{\mu}$

Governing equations

Based on the preceding arguments, the conservation equations are written in Cartesian coordinates as follows[31].

$$\frac{\partial u}{\partial x} + \frac{\partial v}{\partial y} = 0 \quad \ldots (1)$$

$$\rho\left(\frac{\partial u}{\partial t} + u\frac{\partial u}{\partial x} + v\frac{\partial u}{\partial y}\right) = -\frac{\partial p}{\partial x} + (\mu + k)\left(\frac{\partial^2 u}{\partial x^2} + \frac{\partial^2 u}{\partial y^2}\right) + k\frac{\partial N^*}{\partial y} \quad \ldots (2)$$

$$\rho\left(\frac{\partial v}{\partial t} + u\frac{\partial v}{\partial x} + v\frac{\partial v}{\partial y}\right) = -\frac{\partial p}{\partial y} + (\mu + k)\left(\frac{\partial^2 v}{\partial x^2} + \frac{\partial^2 v}{\partial y^2}\right) - k\frac{\partial N^*}{\partial x} - \sigma B_0^2 v + \rho g\beta(T - T_c) \quad \ldots (3)$$

$$\rho\left(\frac{\partial N^*}{\partial t} + u\frac{\partial N^*}{\partial x} + v\frac{\partial N^*}{\partial y}\right) = \gamma\left(\frac{\partial^2 N^*}{\partial x^2} + \frac{\partial^2 N^*}{\partial y^2}\right) - 2kN^* + k\left(\frac{\partial v}{\partial x} - \frac{\partial u}{\partial y}\right) \quad \ldots (4)$$

$$\frac{\partial T}{\partial t} + u\frac{\partial T}{\partial x} + v\frac{\partial T}{\partial y} = \alpha\left(\frac{\partial^2 T}{\partial x^2} + \frac{\partial^2 T}{\partial y^2}\right) \quad \ldots (5)$$

Boundary conditions

The following initial boundary conditions are prescribed at the walls of the enclosure:

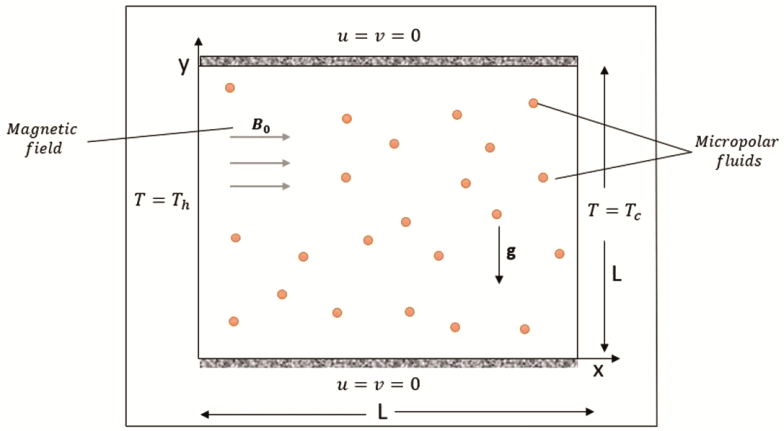

Fig. 1 — Schematic diagram of the physical model

$t = 0 \;\; u = v = T = N = 0 \;\; for \; 0 \le x \le 1$
and $0 \le y \le 1$

$t > 0 \;\; u = v = 0, \qquad \frac{\partial T}{\partial y} = N = 0 \; at \; y = 0,1$

$u = v = 0, T = T_h, \;\; N = 0 \;\; at \quad x = 0$

$u = v = 0, \; T = T_c, \quad N = 0 \quad at \quad x = 1$ … (6)

To transform the Eqs (1)-(5) into non-dimensional form, the following non-dimensional quantities are addressed[14].

$$\tau = \frac{t \propto}{L^2}, \quad X = \frac{x}{L}, \quad Y = \frac{y}{L}, \; U = \frac{uL}{\propto}, \quad V = \frac{vL}{\propto},$$
$$\theta = \frac{T - T_c}{T_h - c}, \quad N = \frac{\eta L^2}{\propto} \qquad \ldots (7)$$

The interpreted equations are given as follows:

$$\frac{\partial U}{\partial X} + \frac{\partial V}{\partial Y} = 0 \qquad \ldots (8)$$

$$\frac{\partial U}{\partial \tau} + U\frac{\partial U}{\partial X} + V\frac{\partial U}{\partial Y} = -\frac{\partial P}{\partial X} + (1 + K)$$
$$Pr\left[\frac{\partial^2 U}{\partial X^2} + \frac{\partial^2 U}{\partial Y^2}\right] + KPr\frac{\partial N}{\partial Y} \qquad \ldots (9)$$

$$\frac{\partial V}{\partial \tau} + U\frac{\partial V}{\partial X} + V\frac{\partial V}{\partial Y} = -\frac{\partial P}{\partial Y} + (1 + K)$$
$$Pr\left[\frac{\partial^2 V}{\partial X^2} + \frac{\partial^2 V}{\partial Y^2}\right] - KPr\frac{\partial N}{\partial X} - \mathrm{Pr}Ha^2V + \mathrm{RaPr}\theta \qquad \ldots (10)$$

$$\frac{\partial N}{\partial \tau} + U\frac{\partial N}{\partial X} + V\frac{\partial N}{\partial Y} = \left(1 + \frac{K}{2}\right)Pr\left[\frac{\partial^2 N}{\partial X^2} + \frac{\partial^2 N}{\partial Y^2}\right] -$$
$$2KNPr + KPr\left(\frac{\partial V}{\partial X} - \frac{\partial U}{\partial Y}\right) \qquad \ldots (11)$$

$$\frac{\partial \theta}{\partial \tau} + U\frac{\partial \theta}{\partial X} + V\frac{\partial \theta}{\partial Y} = \frac{\partial^2 \theta}{\partial X^2} + \frac{\partial^2 \theta}{\partial Y^2} \qquad \ldots (12)$$

Nusselt number

Along the heated wall, the local Nusselt number is defined as:

$$Nu = \frac{hL}{k} \qquad \ldots (13)$$

Here, h represents the heat transfer coefficient that can be denoted as

$$h = \frac{q}{T_h - T_c} \qquad \ldots (14)$$

where q is the rate of heat flux for unit area.

As a result, the local Nusselt number along the left wall can be specified as

$$Nu = -k\frac{T_h - T_c}{L}\frac{\partial \theta}{\partial X}\Big|_{wall} \qquad \ldots (15)$$

Numerical simulation for FVM and grid independent study

The conservation Eqs (8) - (11) which are dimensionless using the boundary condition (6) would have been established with Versteeg and Malalasekra[32] Finite Volume Method (FVM). To ensure a stable and convergent solution, a staggered grid design is employed. In the current computation, a uniform grid system is utilized (Fig. 2), where the distance between nodes is maintained as a consistent length (h).

Discretized X-momentum convection term

$$\iint_V \left(\frac{\partial (UU)}{\partial X} + \frac{\partial (UV)}{\partial Y}\right) dV = \left[\frac{(UU)_e - (UU)_w}{\delta x_u} + \frac{(UV)_n - (UV)_s}{\delta x_y}\right] \Delta V \Delta t \qquad \ldots (16)$$

Where,

$$U_e = \frac{U_{i+1,j} + U_{i,j}}{2}, \; U_n = \frac{U_{i,j} + U_{i,j+1}}{2},$$
$$U_s = \frac{U_{i,j} + U_{i,j-1}}{2}, \; V_n = \frac{V_{i,j} + V_{i+1,j}}{2}, \; V_s = \frac{V_{i,j-1} + V_{i+1,j-1}}{2} \qquad \ldots (17)$$

The nodes e, w, n, s represents the directions east, west, north, south respectively.

In the preceding statement, the subscripts i and j designate the grid locations in the X and Y directions, respectively.

Applying Eq. (17) into the X-direction momentum conservation Eq. (16) leads to the following:

$$\iint_V \left(\frac{\partial (UU)}{\partial X} + \frac{\partial (UV)}{\partial Y}\right) dV = h(U_eU_e - U_wU_w + U_nV_n - U_sV_s) \qquad \ldots (18)$$

Discretized X-momentum diffusion term

$$\left(\iint_V \frac{\partial}{\partial X}\left(\frac{\partial U}{\partial X}\right) + \iint_V \frac{\partial}{\partial Y}\left(\frac{\partial U}{\partial Y}\right)\right) dV = \left[\frac{\left(\frac{\partial U}{\partial X}\right)_e - \left(\frac{\partial U}{\partial X}\right)_w}{\delta x_u} + \frac{\left(\frac{\partial U}{\partial Y}\right)_n - \left(\frac{\partial U}{\partial Y}\right)_s}{\delta y_u}\right] \Delta V \Delta t \qquad \ldots (19)$$

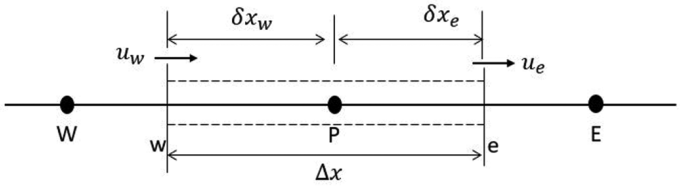

Fig. 2 — Grid generation

Where,

$$\left(\frac{\partial U}{\partial X}\right)_{\boldsymbol{e}}=\frac{U_{i+1,j}-U_{i,j}}{\Delta x}\ \left(\frac{\partial U}{\partial X}\right)_{w}=\frac{U_{i,j}-U_{i-1,j}}{\Delta x}$$
$$\left(\frac{\partial U}{\partial Y}\right)_{n}=\frac{U_{i,j+1}-U_{i,j}}{\Delta y}\ \left(\frac{\partial U}{\partial Y}\right)_{\boldsymbol{s}}=\frac{U_{i,j}-U_{i,j-1}}{\Delta y} \quad \ldots (20)$$

The correct predicted velocities of X-momentum equation,

$$\mathrm{U_p^{n+1}}=U_p^*-\Delta t\left(\frac{P_{i+1}-P_{i,j}}{\Delta x}\right) \quad \ldots (21)$$

Combining the convection and diffusion terms of Eqns. (18), (19) and (20) we obtain the following final X-momentum conservation equation.

$$U_p^*=U_p^n+\Delta t\left[-\frac{1}{h}(U_eU_e-U_wU_w+U_nV_n-U_sV_s)+\frac{(1+K)Pr}{h^2}\left(U_E+U_w+U_N+U_S-4U_p\right)+f_{bx}\right] \quad \ldots (22)$$

Similarly,

Discretized Y-momentum convection term

$$\iint_V\left(\frac{\partial(UV)}{\partial X}+\frac{\partial(VV)}{\partial Y}\right)dV=\left[\frac{(UV)_e-(UV)_w}{\delta x_v}+\frac{(VV)_n-(VV)_s}{\delta x_v}\right]\Delta V\Delta t \quad \ldots (23)$$

Where,

$$U_e=\frac{U_{i,j}+U_{i,j+1}}{2},\ U_w=\frac{U_{i-1,j+1}+U_{i-1,j}}{2},\ V_e=\frac{V_{i,j}+V_{i+1,j}}{2},$$
$$V_w=\frac{V_{i,j}+V_{i-1,j}}{2}\ V_n=\frac{V_{i,j}+V_{i,j+1}}{2},\quad V_s=\frac{V_{i,j}+V_{i,j-1}}{2} \quad \ldots (24)$$

Applying Eq. (24) into the X-direction momentum conservation Eqn. (23) leads to the following:

$$\iint_V\left(\frac{\partial(UV)}{\partial X}+\frac{\partial(VV)}{\partial Y}\right)dV=h(U_eV_e-U_wV_w+V_nV_n-V_sV_s) \quad \ldots (25)$$

Discretized Y-momentum diffusion term

$$\left(\iint_{\boldsymbol{V}}\frac{\partial}{\partial X}\left(\frac{\partial V}{\partial X}\right)+\iint_{\boldsymbol{V}}\frac{\partial}{\partial Y}\left(\frac{\partial V}{\partial Y}\right)\right)dV=\left[\frac{\left(\frac{\partial V}{\partial X}\right)_{\boldsymbol{e}}-\left(\frac{\partial V}{\partial X}\right)_{\boldsymbol{w}}}{\delta\boldsymbol{x_v}}+\frac{\left(\frac{\partial V}{\partial Y}\right)_{\boldsymbol{n}}-\left(\frac{\partial V}{\partial Y}\right)_{\boldsymbol{s}}}{\delta\boldsymbol{y_v}}\right]\Delta V\Delta t \quad \ldots (26)$$

Where,

$$\left(\frac{\partial V}{\partial X}\right)_{\boldsymbol{e}}=\frac{V_{i+1,j}-V_{i,j}}{\Delta x}\left(\frac{\partial V}{\partial X}\right)_{w}=\frac{V_{i,j}-V_{i-1,j}}{\Delta x}\left(\frac{\partial V}{\partial Y}\right)_{n}$$
$$=\frac{V_{i,j+1}-V_{i,j}}{\Delta y}\ \left(\frac{\partial V}{\partial Y}\right)_{\boldsymbol{s}}=\frac{V_{i,j}-V_{i,j-1}}{\Delta y} \quad \ldots (27)$$

The correct predicted velocities of Y-momentum equation,

$$\mathrm{V_p^{n+1}}=V_p^*-\Delta t\left(\frac{P_{i+1}-P_{i,j}}{\Delta y}\right) \quad \ldots (28)$$

Combining the convection and diffusion terms of Eqns. (25), (27) and (28) we obtain the following final Y-momentum conservation equation.

$$V_p^*=V_p^n+\Delta t\left[-\frac{1}{h}(V_eV_e-V_wV_w+V_nV_n-V_sV_s)+\frac{(1+K)Pr}{h^2}\left(V_E+V_w+V_N+V_S-4V_p\right)+f_{by}\right] \quad \ldots (29)$$

Discretization of Micro-rotation Equation

Convection term

$$\iint_V\left(\frac{\partial(UN)}{\partial X}+\frac{\partial(VN)}{\partial Y}\right)dV=\left[\frac{(UN)_e-(UN)_w}{\delta x_v}+\frac{(VN)_n-(VN)_s}{\delta x_v}\right]\Delta V\Delta t \quad \ldots (30)$$

Where,

$$U_e=\frac{U_{i+1,j}+U_{i,j}}{2},\quad U_w=\frac{U_{i-1,j+1}+U_{i-1,j}}{2},\quad V_s=\frac{V_{i,j}+V_{i,j-1}}{2},$$
$$V_n=\frac{V_{i,j}+V_{i+1,j}}{2}\ N_e=\frac{N_{i,j-1}+N_{i+1,j}}{2}\ N_w=\frac{N_{i,j}+N_{i-1,j}}{2},$$
$$N_n=\frac{N_{i,j}+N_{i,j+1}}{2},\ N_s=\frac{N_{i,j}+N_{i,j-1}}{2} \quad \ldots (31)$$

Diffusion term

$$\left(\iint_{\boldsymbol{V}}\frac{\partial}{\partial X}\left(\frac{\partial N}{\partial X}\right)+\iint_{\boldsymbol{V}}\frac{\partial}{\partial Y}\left(\frac{\partial N}{\partial Y}\right)\right)dV=\left[\frac{\left(\frac{\partial N}{\partial X}\right)_{\boldsymbol{e}}-\left(\frac{\partial N}{\partial X}\right)_{\boldsymbol{w}}}{\delta\boldsymbol{x_u}}+\frac{\left(\frac{\partial N}{\partial Y}\right)_{\boldsymbol{n}}-\left(\frac{\partial N}{\partial Y}\right)_{\boldsymbol{s}}}{\delta\boldsymbol{y_u}}\right]\Delta V\Delta t \quad \ldots (32)$$

$$\left(\frac{\partial N}{\partial X}\right)_{\boldsymbol{e}}=\frac{N_{i+1,j}-N_{i,j}}{\Delta x}\left(\frac{\partial N}{\partial X}\right)_{w}=\frac{N_{i,j}-N_{i-1,j}}{\Delta x}$$
$$\left(\frac{\partial N}{\partial Y}\right)_{n}=\frac{N_{i,j+1}-N_{i,j}}{\Delta y}\left(\frac{\partial N}{\partial Y}\right)_{\boldsymbol{s}}=\frac{N_{i,j}-N_{i-1,j-1}}{\Delta y} \quad \ldots (33)$$

Applying Eq. (31) and (33) into the micro-rotation Eq. (4) the final combined equation leads the following:

$$N_p^*=N_p^n+\Delta t\left[-\frac{1}{h}(U_eN_e-U_wN_w+V_nN_n-V_sN_s)+\frac{(1+K)Pr}{h^2}(N_E+N_w+N_N+N_S-4N)+f_{bN}\right] \quad \ldots (34)$$

Discretization of Energy Equation

Convection term

$$\iint_V\left(\frac{\partial(U\theta)}{\partial X}+\frac{\partial(V\theta)}{\partial Y}\right)dV=\left[\frac{(U\theta)_e-(U\theta)_w}{\delta x_v}+\frac{(V\theta)_n-(V\theta)_s}{\delta x_v}\right]\Delta V\Delta t \quad \ldots (35)$$

$$U_e=\frac{U_{i+1.j}}{2},\quad U_w=\frac{U_{i.j}}{2},\quad V_n=\frac{V_{i.j+1}}{2},$$
$$V_s=\frac{V_{i.j}}{2}, \quad \ldots (36)$$

Diffusion term

$$\left(\iint_V \frac{\partial}{\partial X}\left(\frac{\partial \theta}{\partial X}\right) + \iint_V \frac{\partial}{\partial Y}\left(\frac{\partial \theta}{\partial Y}\right)\right) dV = \left[\frac{\left(\frac{\partial \theta}{\partial X}\right)_e - \left(\frac{\partial \theta}{\partial X}\right)_w}{\delta x_u} + \frac{\left(\frac{\partial \theta}{\partial Y}\right)_n - \left(\frac{\partial \theta}{\partial Y}\right)_s}{\delta y_u}\right] \Delta V \Delta t \quad \ldots (37)$$

$$\left(\frac{\partial \theta}{\partial X}\right)_e = \frac{\theta_{i+1,j} - \theta_{i,j}}{\Delta x} \left(\frac{\partial \theta}{\partial X}\right)_w = \frac{\theta_{i,j} - \theta_{i-1,j}}{\Delta x} \left(\frac{\partial \theta}{\partial Y}\right)_n = \frac{\theta_{i,j+1} - \theta_{i,j}}{\Delta y} \left(\frac{\partial \theta}{\partial Y}\right)_s = \frac{\theta_{i,j} - \theta_{i-1,j-1}}{\Delta y} \quad \ldots (38)$$

Applying Eq. (36) and (38) into the energy Eq. (5) the final combined equation leads the following:

$$\theta_p^* = \theta_p^n + \Delta t \left[-\frac{1}{h}(U_e\theta_e - U_w\theta_w + V_n\theta_n - V_s\theta_s) + \frac{(1+K)Pr}{h^2}\left(\theta_E + \theta_w + \theta_N + \theta_S - 4\theta_p\right) + f_{b\theta}\right] \quad \ldots (39)$$

Validation of numerical results

To validate the numerical results utilized in the present analysis through the finite volume method, accuracy and validity checks are essential. Table 2 shows the average Nusselt number values, computed for varying Rayleigh numbers are displayed alongside comparisons to values reported by other researchers. Upon reviewing the tables, it is evident that there is a strong agreement between the results. Thus, these favourable comparisons significantly gives confidence in the reported results.

To ensure a grid-independent solution, a sensitivity analysis of the grid was conducted. The grid-independent solution was attained by configuring the solution for unsteady free convection within a square cavity containing a micropolar fluid under the conditions: Ra = 10^5, Pr = 0.7, K = 0.5, Ha=50.

Table 2 — Comparison of the average Nusselt number of the hot wall

Ra	K	Aydin & Pop[11]	Zadravec *et al.*[4]	Sheremet *et al.*[7]	Present study
10^3	0	1.118	1.118	1.118	1.117
	0.5	1.057	1.059	1.059	1.058
	2.0	1.016	1.017	1.016	1.019
10^4	0	2.234	2.263	2.245	2.265
	0.5	1.947	1.986	1.977	1.988
	2.0	1.545	1.578	1.566	1.566
10^5	0	4.486	4.540	4.529	4.479
	0.5	4.033	4.067	4.081	4.043
	2.0	3.314	3.377	3.348	3.327
10^6	0	8.945	8.742	8.841	8.857
	0.5	7.984	8.229	8.187	7.983
	2.0	6.673	6.714	6.875	6.672

Results and Discussion

Extensive work has been conducted through Finite Volume Method (FVM) simulations to illustrate the transport characteristics within the enclosure. The relevant parameter values are set within the specified ranges as follows: Rayleigh number $10^3 \leq Ra \leq 10^5$, Hartmann number $0 \leq Ha \leq 50$ and Vortex viscosity parameter $(0 \leq K \leq 5)$. For all simulations the Prandtl number $(Pr = 0.71)$ is considered. Flow patterns are observed through the visualization of streamlines, while temperature fields are depicted using isotherm contours.In addition, Fig. 3 shows the modelling and numerical simulations comparisons to Asadi *et al.*[30] work to confirm the micropolar fluid effects. In this comparison for two different values of vortex viscosity parameter (K =0.5 & 1) This ensures that the results of present study strongly agree to the existing work.

Influence of Hartmann number on streamlines and isotherms

Figs 4(a)-(d) depict the influence of the magnetic field parameter. The Hartmann number has a substantial impact on fluid movement and heat convection. Fig. 4(a) shows that when Ha is absent, convection is increased. In Fig. 4(b), when Ha=10 the streamlines are largely symmetric and the profiles formed are very closer at the top of the cavity while the profiles symmetrically enlarged towards the bottom of the wall. The temperature in the middle of the cavity seems colder and the heat generates at the bottom of the cavity. The left wall, kept at a high temperature, generates a vortex at the lower-left corner. The results remain consistent at all stages as the Hartmann number increases. With increasing Hartmann number, the streamlines and eddies remain unchanged. However, when analyzing the isotherms, as the Hartmann number increases, the eddies in the cavity stretch more towards the top of the cold vertical wall. Additionally, as the temperature decreases, the size of the isotherm lines within the eddies continuously decreases downward towards the vertical bottom wall.

Influence of Rayleigh number on streamlines and isotherms

Fig. 5 depicts the related flow fields and temperature distribution of streamlines and isotherms. In Fig. 5(a) the emergence of convective core areas are colder and the profiles formed in the enclosure are enlarged and the temperature increases gradually towards the bottom wall of the cavity. The regimes are closer together on the top vertical wall. Additionally,

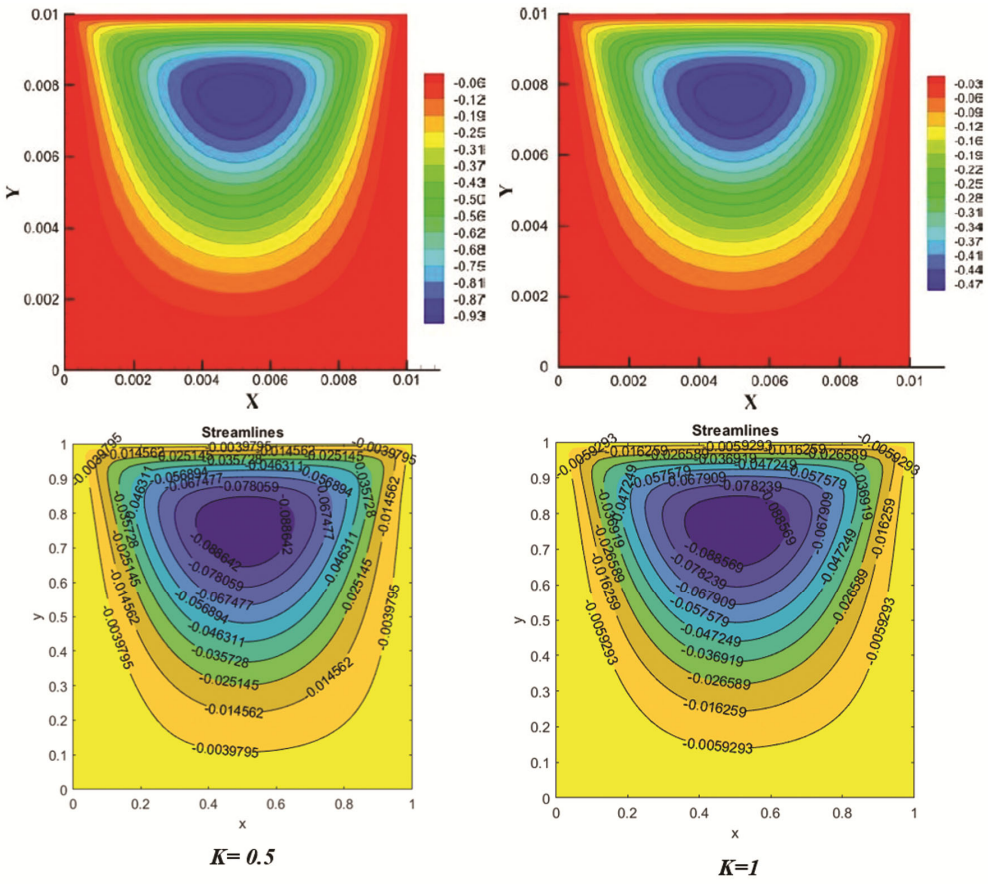

Fig. 3 — Comparison for streamlines between present work (right column) and Asadi *et al.*[33] (left column) for K = 0.5 and K = 1 at $Ra = 10^2$, Pr=0.71

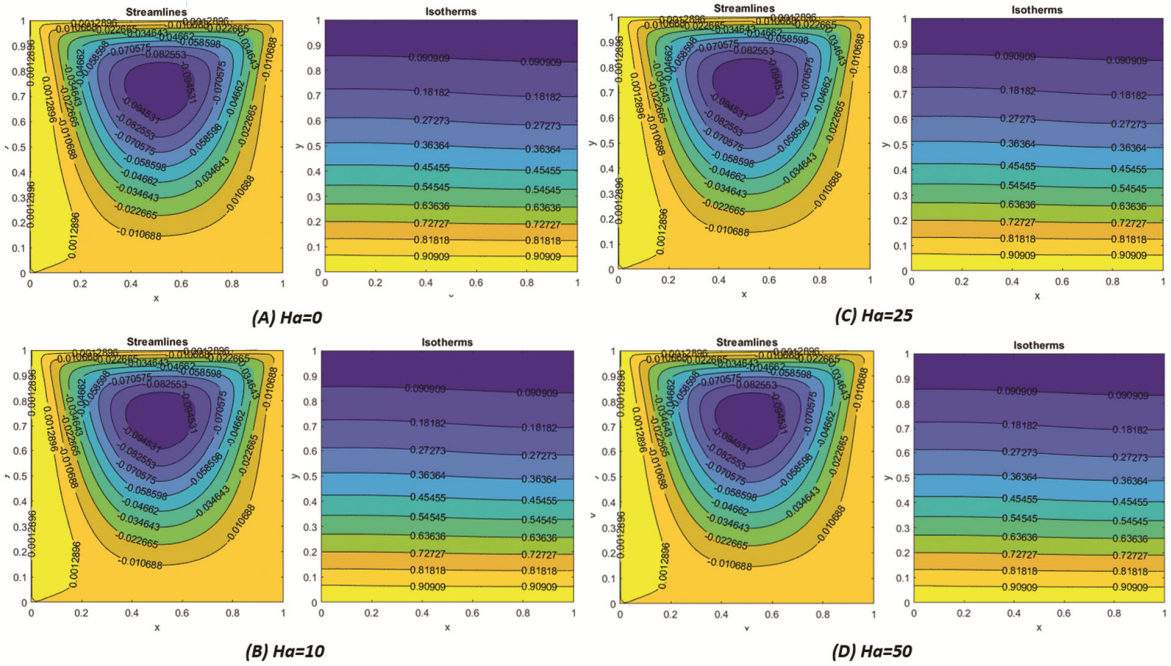

Fig. 4 — Streamlines and isotherms for $Pr = 0.71, Ra = 10^3,\ K = 1$ and different values of Hartmann number (a) Ha=0, (b) Ha=10, (c) Ha=25 and (d) Ha=50

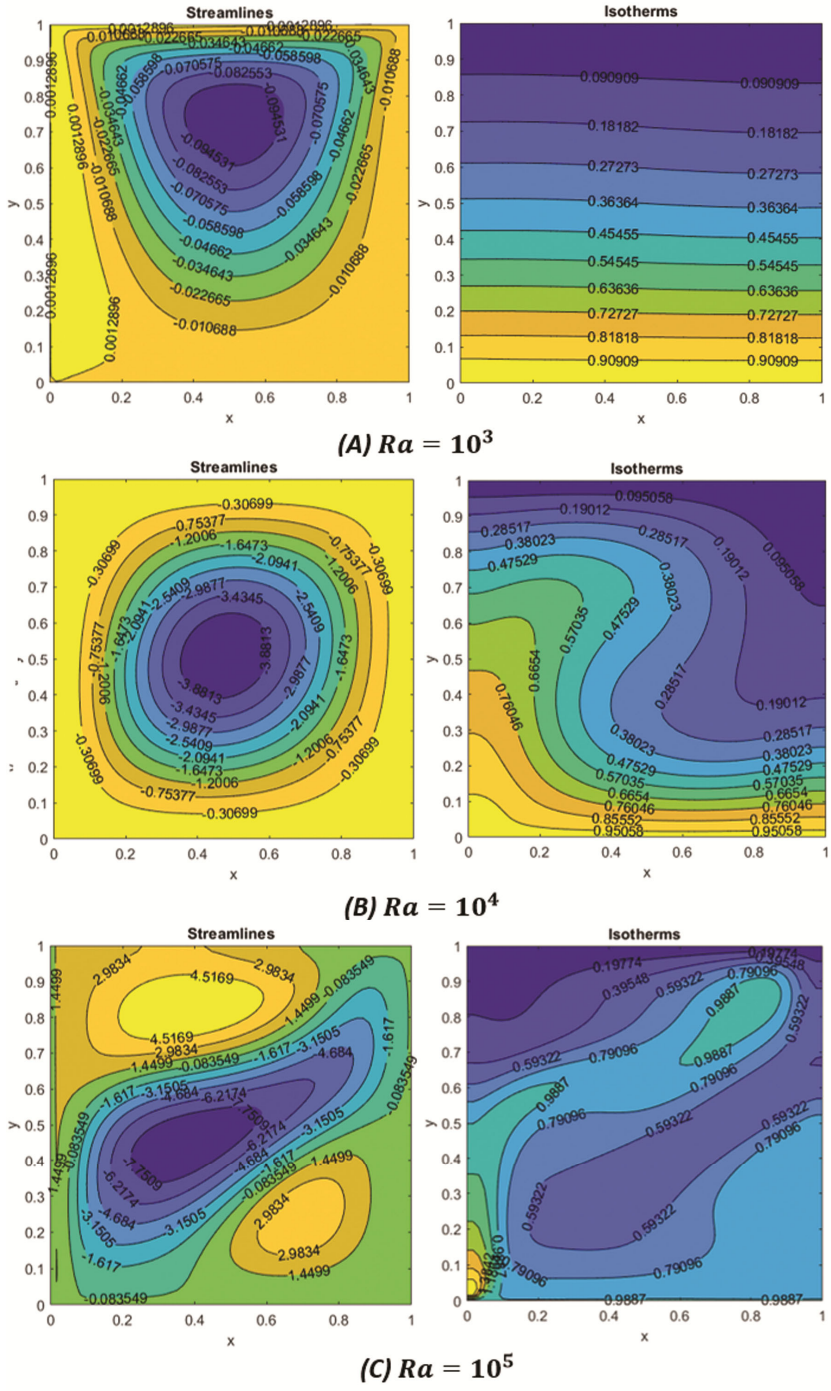

Fig. 5 — Streamlines and isotherms for $Pr = 0.71, Ha = 10$, $K=1$ and different values of Rayleigh number $(A)Ra = 10^3 (B)Ra = 10^4$ $(C)Ra = 10^5$

the flow regimes near the left vertical corner wall are narrow within the cavity, while those near the bottom left corner wall are laterally elongated. In addition, For Ra = 10^3 the isotherm profiles are colder at the top of the eddies and gradually move closer to the bottom of the walls. In Fig. 5(b) for $Ra = 10^4$, the streamlines generate symmetric contours and seems uniformly throughout the region. According to isotherms the lines distorted, curved and twisted more at the corner of the walls when comparing to the center of the cavity. When $Ra = 10^5$, Fig. 5(c) shows new streamline cells evolving at the center

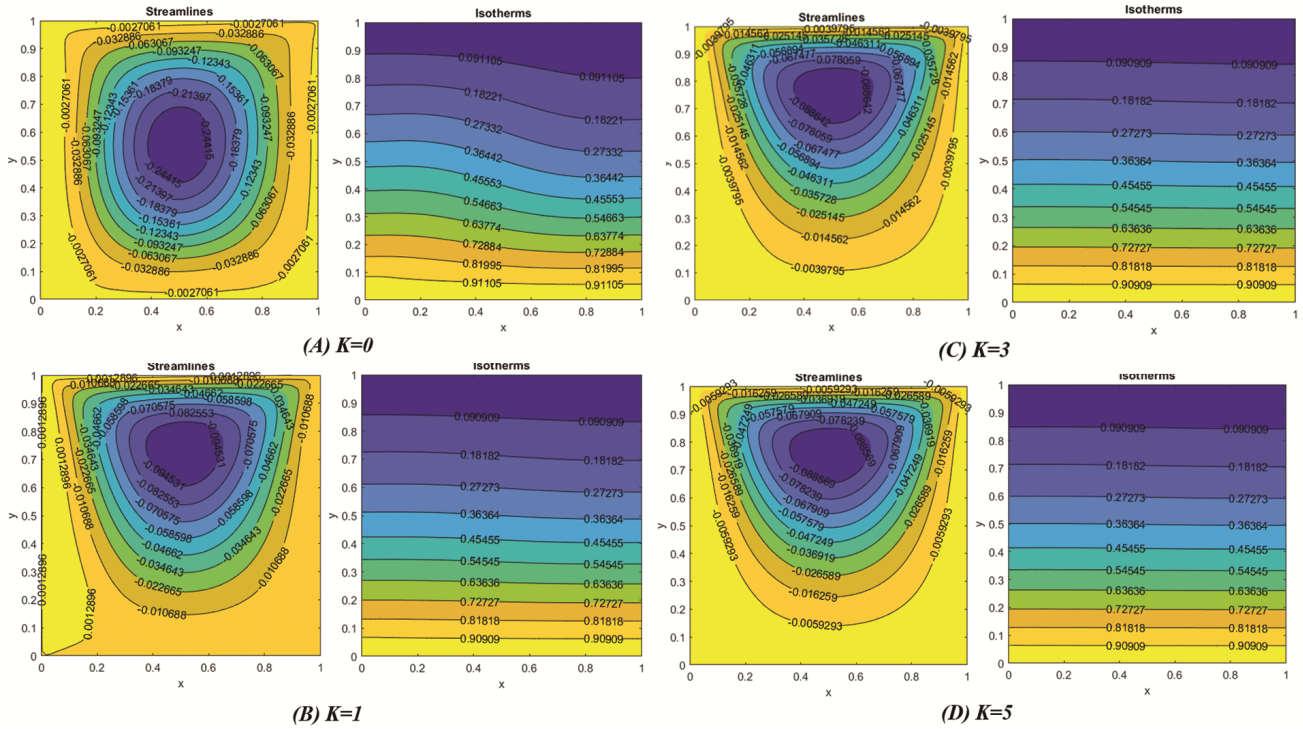

Fig. 6 — Streamlines and isotherms for$Pr = 0.71, Ha = 10,\ Ra = 10^3$and different values of Rayleigh number $(A)K = 0\ \ (B)K = 1\ \ (C)K = 3\ \ (D)K = 5$

with cool temperature and two cells newly formed on top of cold cells while another one at the bottom of the cold cell. When considering with isotherms the contours distorted completely.

Influence of Vortex viscosity parameter on streamlines and isotherms

Fig. 6 illustrates the impact of the vortex viscosity parameter on the flow patterns within the cavity, as represented by streamlines and isotherms for various values of $0 \leq K \leq 5$. In the lack of vertex viscosity for K=0 (Fig. 6a) the isotherms contours are spreads from hot wall to cold walls and the streamlines formed in the eddies are symmetric and uniform. As increasing the vortex viscosity parameter, i.e., K=1 (Fig. 6b) the eddies generated nearby in the top of the cavity can be observed reaching from one side to the left vertical wall. When K=3, 5 (Fig. 6c & 6d) the contour of the streamlines seems similar and the values of those streamlines increase gradually. When taking isotherms for K=0 (Fig. 5A) the profiles generated at the top of the wall and elaborated and suddenly it narrows down towards the bottom of the wall. For K=1, 3, 5 (Fig. 6b-d) the contour approaches similar results and developing symmetric lines in the cavity.

Conclusion

In this study, numerical simulations using the Finite Volume Method were employed to model the magnetohydrodynamic natural convection flow within a two-dimensional, unsteady, laminar, and incompressible micropolar fluid confined within a square cavity. The investigation reveals that a stronger magnetic field results in a decrease in both the flow rate and the rate of heat distribution. The above correlation provides the magnetic field influence on the Rayleigh number and the associated fluid dynamics and heat transfer processes The vortex viscosity parameter significantly influences the flow dynamics and heat transfer characteristics of micropolar fluids. Higher values of the vortex viscosity parameter enhance the coupling between micro-rotational effects and the translational motion of fluid particles. The presence of the vortex viscosity parameter influences the configuration and curvature of streamlines in the fluid flow domain. Higher values of the vortex viscosity parameter enhance the coupling between micro-rotational effects and the translational motion of fluid particles, leading to improved heat transfer and altered fluid behaviour. These findings provide valuable insights for the design and optimization of

industrial heat transfer devices and heat recovery systems. This research underscores the importance of integrating these advanced fluids and magnetic field techniques to achieve superior thermal efficiency and operational stability in real-world industrial settings.

Nomenclature

Symbol	Description
B_0	Induced magnetic field
C_p	Specific heat
g	Gravitational acceleration
T_c	Temperature at cold wall
N	Dimensional microrotation angular velocity
κ	Vortex viscosity parameter
L	Length of the enclosure
Ra	Rayleigh number
N^*	Dimensionless microrotation angular velocity
Ha	Hartman nnumber
K	Dimensionless vortex viscosity parameter
Pr	Prandtl number
t	Time
T	Temperature
X	Non-dimensional coordinate in horizontal direction
u	Dimensional velocity component in X-direction
V	Non-dimensional velocity component in Y-direction
y	Cartesian coordinate in vertical direction
U	Non-dimensional velocity component in X-direction
p	Pressure
Y	Non-dimensional coordinate in vertical direction
v	Dimensional velocity component in y-direction
T_h	Temperature at hot wall
x	Cartesian coordinate in horizontal direction
i,j	Grid location in X, Y directions
Nu	Local Nusselt number
Symbol	**Geek Letters**
γ	Spin-gradient viscosity
ρ	Fluid density
μ	Dynamic viscosity
τ	Non-dimensional time
α	Thermal diffusivity
θ	Non-dimensional temperature
η	Non-dimensional angular momentum
E, W, N, S	East, West, North, South — Nodes
e, w, n, s	East, West, North, South —faces

References

1 Eringen A C, Simple micro fluids, *Int J Eng Sci*, 2 (1964) 205.

2 Saleem M, Asghar S & Hossain M A, Natural convection flow of micropolar fluid in a rectangular cavity heated from below with cold sidewalls, *Math Comput Model*, 54 (2011) 508.

3 Gibanov N S, Sheremet M A & Pop I, Natural convection of micropolar fluid in a wavy differentially heated cavity, *J Mol Liq*, 221 (2016) 518.

4 Zadravec M, Hriberšek M & Škerget L, Natural convection of micropolar fluid in an enclosure with boundary element method, *Eng Anal Bound Elem*, 33 (2009) 485.

5 Sheikholeslami M, Hatami M & Ganji D D, Micropolar fluid flow and heat transfer in a permeable channel using analytical method, *J Mol Liq*, 194 (2014) 30.

6 Javed T & Siddiqui M A, Energy transfer through mixed convection within square enclosure containing micropolar fluid with non-uniformly heated bottom wall under the MHD impact, *J Mol Liq*, 249 (2018) 831.

7 Sheremet M A, Pop I & Ishak A, Time-dependent natural convection of micropolar fluid in a wavy triangular cavity, *Int J Heat Mass Transf*, 105 (2017) 610.

8 Ariman T, Turk M A & Sylvester N D, Applications of microcontinuum fluid mechanics, *Int J Eng Sci*, 12 (1974) 273.

9 Yoshida M & Hamano Y, Numerical studies on the dynamics of two-layer Rayleigh-Bénard convection with an infinite Prandtl number and large viscosity contrasts, *Phys Fluids*, 28 (2016) 116601.

10 Tso C P, Jin L F, Tou S K W & Zhang X F, Flow pattern evolution in natural convection cooling from an array of discrete heat sources in a rectangular cavity at various orientations, *Int J Heat Mass Transf*, 47 (2004) 4061.

11 Aydin O & Pop I, Natural convection in a differentially heated enclosure filled with a micropolar fluid, *Int J Therm Sci*, 46 (2007) 963.

12 Frederick J H, Fujiwara Y, Penn J H, Yoshihara K & Petek H, Models for stilbene photoisomerization: Experimental and theoretical studies of the excited-state dynamics of 1,2-diphenylcycloalkenes, *J Phys Chem*, 95 (1991) 2845.

13 Bilgen E, Natural convection in cavities with a thin fin on the hot wall, *Int J Heat Mass Transf*, 48 (2005) 3493.

14 Hsu T, Natural convection of micropolar fluids in an enclosure with heat sources, *Int J Heat Mass Transf*, 40 (1997) 4239.

15 Gibanov N S, Sheremet M A & Pop I, Free convection in a trapezoidal cavity filled with a micropolar fluid, *Int J Heat Mass Transf*, 99 (2016) 831.

16 Miroshnichenko I V, Sheremet M A & Pop I, Natural convection in a trapezoidal cavity filled with a micropolar fluid under the effect of a local heat source, *Int J Mech Sci*, 120 (2017) 182.

17 Basak T, Roy S & Balakrishnan A R, Effects of thermal boundary conditions on natural convection flows within a square cavity, *Int J Heat Mass Transf*, 49 (2006) 4525.

18 Khanafer K M, Al-amiri A M & Pop I, Numerical simulation of unsteady mixed convection in a driven cavity using an externally excited sliding lid, *Europ J Mech B/Fluids*, 26 (2007) 669.

19 Barth T J, Aspects of unstructured grids and finite-volume solvers for the euler and navier-stokes equations, *Fluids Mech Heat Transf*, (1992) 1.

20 Huang Q M, Ren Y X & Wang Q, High order finite volume schemes for solving the non-conservative convection equations on the unstructured grids, *J Sci Comput*, 88 (2021).

21 Nishikawa H, The quick scheme is a third-order finite-volume scheme with point-valued numerical solutions, *Int J Numer Methods Fluids*, 93 (2021) 2311.

22 Patel M R & Pandya J U, A research study on unsteady state convection diffusion flow with adoption of the finite volume technique, *J Appl Math Comput Mech*, 20 (2021) 65.

23 Busto S, Dumbser M, Gavrilyuk S & Ivanova K, On thermodynamically compatible finite volume methods and

path-conservative ADER discontinuous Galerkin schemes for turbulent shallow water flows, *J Sci Comput*, 88 (2021) 1.

24 Cao X & Huang H, An adaptive conservative finite volume method for poisson-nernst-planck equations on a moving mesh, *Commun Comput Phys*, 26 (2019) 389.

25 Durlofsky L J, Efendiev Y & Ginting V, An adaptive local-global multiscale finite volume element method for two-phase flow simulations, *Adv Water Resour*, 30 (2007) 576.

26 Balaji N, Nithyanandan N, Adalarasan R, Santhanakumar M & Kumar P S M, Scalable parallel finite volume lattice Boltzmann method for thermal incompressible flows on unstructured grids, *J New Mater Electrochem Syst*, 21 (2018) 141.

27 Prakash R, Kamatchi R, Selvam R & Devanathan C, An adaptive local–global multiscale finite volume element method for two-phase flow simulations, *J Phys: Conf Ser*, 2484 (2023) 012035.

28 Acharya N & Oztop H F, Finite element simulation of micropolar fluidflow in the lid-driven square cavity, *Numer Heat Transf Part A: Appl*, (2023).

29 Acharya N, On the flow patterns and thermal control of radiative natural convective hybrid nanofluid flow inside a square enclosure having various shaped multiple heated obstacles, *Eur Phys J Plus*, 136 (2021) 889.

30 Acharya N, Magnetically driven MWCNT-Fe3O4-water hybrid nanofluidic transport through a micro-wavy channel: A novel MEMS design for drug delivery application, *Mater Today Commun*, 38 (2024) 107844.

31 Vinodhini N & Prasad V R, Magneto-hybrid nanofluid (Cu−Oil) flow in a porous square enclosure with Cattaneo-christov heat flow model-sensitivity analysis, *Indian J Chem Technol*, 30 (2023) 714.

32 Azimi M & Riazi R, Analytical solution of unsteady GO water nanofluid flow and heat transfer between two parallel moving plates, *Indian J Chem Technol*, 23 (2016) 47.

33 Reddy A S, Challa K K, Srinivas S, Ramamohan T R & Vajravelu K, Influence of ohmic heating and thermal radiation on chemically reactive pulsatile flow of casson nanofluid in a vertical porous channel embeddedin non-Darcy porous medium, *Indian J Chem Technol*, 31 (2024) 186.

34 Nering K & Rup K, The effect of nanoparticles added to heated micropolar fluid, *Superlattices Microstruct*, 98 (2016) 283.

35 Versteeg H K & Malalasekera W, The finite volume method, An Introduction to Computational Fluid Dynamics, (1995) 102.

36 Asadi H, Javaherdeh K & Ramezani S, Finite element simulation of micropolar fluid flow in the lid-driven square cavity, *Int J Appl Mech*, 5 (2013) 1350045.